© 2013. Published by The Company of Biologists Ltd | Development (2013) 140, 4970-4981 doi:10.1242/dev.099192

RESEARCH ARTICLE

N-glycosylation requirements in neuromuscular synaptogenesis

William Parkinson, Mary Lynn Dear, Emma Rushton and Kendal Broadie*

ABSTRACT

Neural development requires N-glycosylation regulation of intercellular signaling, but the requirements in synaptogenesis have not been well tested. All complex and hybrid N-glycosylation requires MGAT1 (UDP-GlcNAc:α-3-D-mannoside-β1,2-N-acetylglucosaminyl-transferase I) function, and *Mgat1* nulls are the most compromised N-glycosylation condition that survive long enough to permit synaptogenesis studies. At the *Drosophila* neuromuscular junction (NMJ), *Mgat1* mutants display selective loss of lectin-defined carbohydrates in the extracellular synaptomatrix, and an accompanying accumulation of the secreted endogenous Mind the gap (MTG) lectin, a key synaptogenesis regulator. Null *Mgat1* mutants exhibit strongly overelaborated synaptic structural development, consistent with inhibitory roles for complex/hybrid N-glycans in morphological synaptogenesis, and strengthened functional synapse differentiation, consistent with synaptogenic MTG functions. Synapse molecular composition is surprisingly selectively altered, with decreases in presynaptic active zone Bruchpilot (BRP) and postsynaptic Glutamate receptor subtype B (GLURIIB), but no detectable change in a wide range of other synaptic components. Synaptogenesis is driven by bidirectional trans-synaptic signals that traverse the glycan-rich synaptomatrix, and *Mgat1* mutation disrupts both anterograde and retrograde signals, consistent with MTG regulation of trans-synaptic signaling. Downstream of intercellular signaling, pre- and postsynaptic scaffolds are recruited to drive synaptogenesis, and *Mgat1* mutants exhibit loss of both classic Discs large 1 (DLG1) and newly defined Lethal (2) giant larvae [L(2)GL] scaffolds. We conclude that MGAT1-dependent N-glycosylation shapes the synaptomatrix carbohydrate environment and endogenous lectin localization within this domain, to modulate retention of trans-synaptic signaling ligands driving synaptic scaffold recruitment during synaptogenesis.

KEY WORDS: Synaptomatrix, Trans-synaptic signaling, Synaptic scaffold, Active zone, Glutamate receptor, Neuromuscular junction, *Drosophila*

INTRODUCTION

N-glycosylation is the most common post-translational modification, involving linkage of diverse carbohydrate trees onto asparagine, targeting primarily cell surface and secreted proteins. Mutation of >20 human N-glycosylation genes result in heritable congenital disorders of glycosylation (CDGs), many of which impair nervous system development (Freeze, 2006; Hennet, 2012; Hewitt, 2009). The *Mgat1* gene encoding GlcNAcT1 adds GlcNAc to high-mannose sites (Schachter, 2010); an essential early step in producing all complex and hybrid N-glycans (Pownall et al., 1992; Ye and Marth, 2004). Thus, MGAT1 generates the entire repertoire of polymeric branched N-glycans destined for secretion or presentation on the cell surface (Puthalakath et al., 1996); and *Mgat1* null mutants, containing high mannose in place of complex/hybrid N-glycans, are the earliest N-glycan pathway block available to study N-glycosylation requirements in neural development (Schachter and Boulianne, 2011). Mouse *Mgat1* knockouts are lethal at embryonic day (E) 9.5, but conditional mutants show movement defects, tremors, paralysis and early death characteristic of neurodevelopmental impairments (Campbell et al., 1995; Grasa et al., 2012; Shi et al., 2004; Ye and Marth, 2004). *Drosophila Mgat1* is functionally conserved, and null mutants show the same range of crippling neurological defects, but have the enormous benefit for analysis of being viable.

Drosophila Mgat1 null mutants exhibit severely impaired coordinated movement, and the few adults that eclose usually survive only a few days (Sarkar et al., 2006). Importantly, lifespan shortening is due entirely to neuron-specific requirements, and *Mgat1* neuronal overexpression increases lifespan (Sarkar et al., 2010; Schachter and Boulianne, 2011). In the central brain mushroom body learning/memory center, *Mgat1* nulls show fused lobes similar to *fused lobes* (*fdl*) mutants in β-N-acetylglucosaminidase, which removes the MGAT1-added GlcNAc (Léonard et al., 2006; Sarkar et al., 2006). MGAT1 is also required for α3 fucose addition, a neuron-specific modification routinely labeled with anti-horseradish peroxidase (HRP) (Desai et al., 1994; Paschinger et al., 2009). Overexpression of the fucose transferase generating HRP glycans increases peripheral sensory neuron clustering, ventral nerve cord growth and glial migration (Rendić et al., 2010). MGAT1-dependent N-glycosylation occurs on many neural proteins, including neurotransmitter receptors, SNAREs, fasciclins, Neuroglian, neurexins and Dystroglycan (Koles et al., 2007; Muntoni et al., 2008; Sun and Xie, 2012).

The heavily glycosylated synaptomatrix is composed of secreted and membrane molecules residing at the interface between presynaptic active zones and postsynaptic receptors. *Drosophila* genetic analyses show synaptomatrix glycan modification/binding has core roles in structural and functional development of the neuromuscular junction (NMJ) synapse (Broadie et al., 2011; Dani and Broadie, 2012). Glycan-dependent synaptogenic events include presynaptic active zone (AZ) differentiation, postsynaptic glutamate receptor (GluR) localization and extracellular matrix (ECM) organization within the synaptic cleft, driven by the secreted endogenous Mind the gap (MTG) lectin, for example (Dani et al., 2012; Long et al., 2008; Rushton et al., 2012). Synaptogenic events are regulated by bidirectional trans-synaptic signals that traverse the synaptomatrix, and glycosylation of both ligands and receptors alters localization and binding (Henríquez and Salinas, 2012; Patton, 2003). Three well-characterized trans-synaptic signals at the *Drosophila* NMJ are the Wnt protein Wingless (WG), the bone morphogentic protein Glass bottom boat (GBB), and Jelly belly (JEB) (Del Grosso et al., 2011; Kamimura et al., 2013; Rohrbough and Broadie, 2010; Tanaka et al., 2002).

Department of Biological Sciences, Kennedy Center for Research on Human Development, Vanderbilt University, Nashville, TN 37212, USA.

*Author for correspondence (kendal.broadie@vanderbilt.edu)

Received 17 May 2013; Accepted 29 September 2013

Development (2013) doi:10.1242/dev.099192

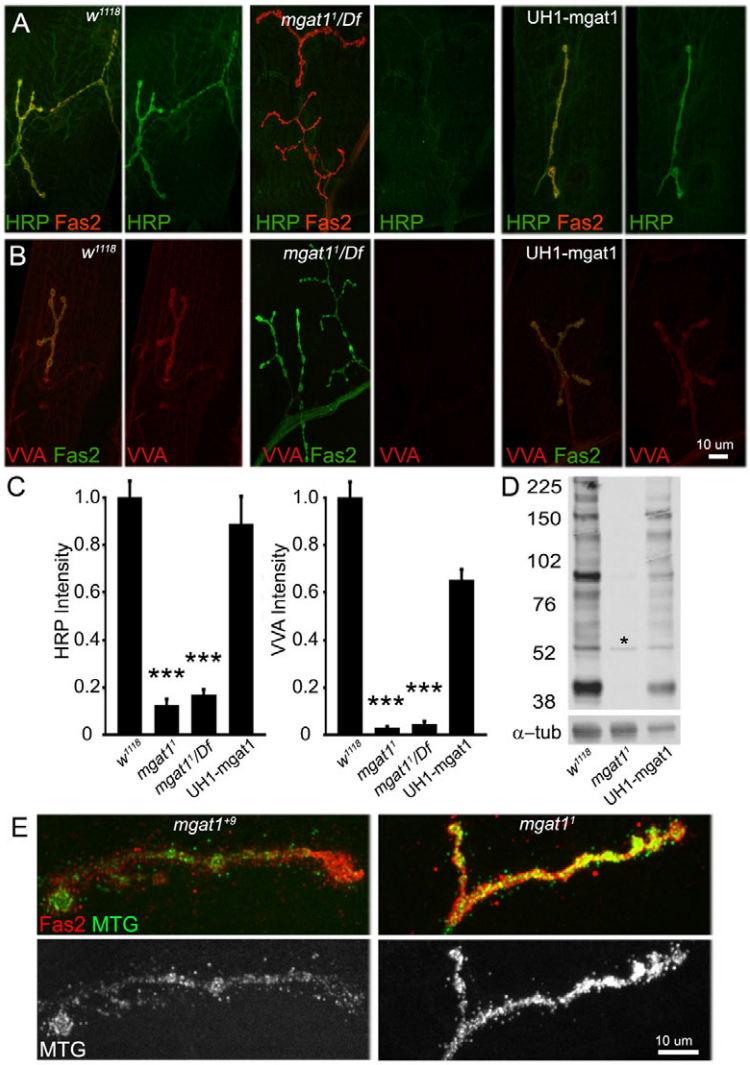

Fig. 1. Loss of *Mgat1* activity dramatically alters the *Drosophila* NMJ synaptomatrix. (A) Representative images of wandering third instar NMJs probed with anti-horseradish peroxidase (HRP, green) and anti-Fasciclin 2 (Fas2, red) in genetic control w^{1118}, $Mgat1^{1}$/Df(2R)BSC430 and UH1-GAL4 driven UAS-*Mgat1* in $Mgat1^{1}$ null background. HRP labeling is undetectable in the *Mgat1* null, and fully restored by the genetic rescue. (B) Representative NMJ images of *Vicia villosa* (VVA, red) lectin labeling with Fas2 co-labeling (green) in the same genotypes. VVA labeling is undetectable in *Mgat1* nulls, and fully restored by genetic rescue. (C) Quantification of HRP and VVA intensity normalized to w^{1118}. ***P≤0.001 (ANOVA). Sample size is ≥10 NMJs from at least five animals of each genotype. (D) Representative anti-HRP western blot from w^{1118}, *Mgat1* null and UH1-*Mgat1* rescue conditions. All HRP glycans are undetectable in *Mgat1* null, and restored by *Mgat1* rescue. The single band (asterisk) represents bleed-through from α-tubulin loading control. (E) Representative NMJ images of Mind the gap (MTG-GFP, green) lectin co-labeled with anti-Fas2 (red), and shown alone (MTG, white), in control ($Mgat1^{+9}$ precise excision) and *Mgat1* null. MTG is greatly increased in mutants (P≤0.0009; sample size: at least eight NMJs, at least four animals/genotype).

The goal here is to test N-glycosylation requirements during NMJ synaptogenesis using *Mgat1* mutants. We found large alterations in synaptomatrix glycan composition, including complete lack of paucimannose glycans, fucosylated HRP epitopes and *Vicia villosa* (VVA) lectin reactivity, coupled to strongly elevated MTG expression. Null *Mgat1* mutants display increased NMJ growth (increased synapse area, branching and bouton number) and function (increased transmission and FM1-43 dye cycling), showing that MGAT1-dependent N-glycosylation plays inhibitory roles in synaptogenesis. Consistent with the hypothesis that a modified synaptomatrix would alter trans-synaptic signaling, WG, GBB and JEB signaling ligands are all disrupted in the absence of *Mgat1* function, together with loss in synaptic recruitment of Discs large 1 (DLG1) and Lethal (2) giant larvae [L(2)GL] membrane scaffolds that modulate NMJ synaptogenesis (Humbert et al., 2008; Staples and Broadie, 2013; Wang et al., 2011). Together, these results show requirements for MGAT1-dependent N-glycosylation in trans-synaptic signaling and synaptic localization of intracellular scaffolds driving neuromuscular synaptogenesis.

RESULTS

MGAT1 shapes the glycosylated synaptomatrix of the NMJ

Lectins have been used to define the specialized carbohydrate environment of pre/postsynaptic membranes and perisynaptic extracellular space (Broadie et al., 2011; Dani and Broadie, 2012). For example, the widely employed anti-HRP antibody binds fucosylated N-glycans in the presynaptic membrane, which require *Mgat1* for fucose modification (Sarkar et al., 2006). Likewise, VVA lectin is a synaptic glycan marker at the *Drosophila* NMJ, which reportedly recognizes primarily postsynaptic Dystroglycan (Haines et al., 2007; Rushton et al., 2012). The endogenous MTG lectin patterns the extracellular glycosylated synaptomatrix (Rohrbough et al., 2007), modulates trans-synaptic signaling and is essential for functional synaptogenesis (Rushton et al., 2009; Rohrbough and Broadie, 2010). To begin to define synaptogenic roles of MGAT1, we labeled the NMJ with each of these lectins in genetic control, *Mgat1* null mutants and *Mgat1* rescue conditions (Fig. 1).

Wandering third instar NMJs were first probed with anti-HRP (green) compared to anti-Fasciclin 2 (FAS2, red) in two *Mgat1* null conditions [$Mgat1^{1}$/$Mgat1^{1}$ and $Mgat1^{1}$/Df(2R)BSC430) compared with w^{1118} genetic control (Fig. 1A)]. The HRP epitope robustly revealed the presynaptic terminal in control, but was undetectable in mutants. Phenotype rescue was assessed with ubiquitous UH1-Gal4 driven UAS-*Mgat1* in the *Mgat1* null background, showing complete recovery of the HRP signal (Fig. 1A, right). Quantification of mutants normalized to the control shows significant loss of HRP signal (w^{1118}: 1.0±0.06; $Mgat1^{1}$: 0.12±0.02, P<0.001; $Mgat1^{1}$/Df: 0.16±0.03.

Development (2013) doi:10.1242/dev.099192

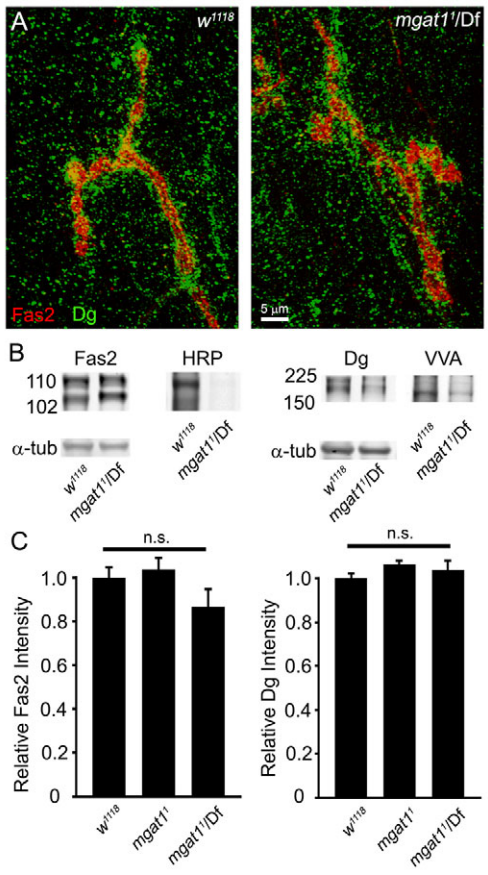

Fig. 2. Fasciclin 2 and Dystroglycan are normally expressed in *Mgat1* nulls. (A) Representative NMJ images of anti-Fasciclin 2 (Fas2, red) double-labeled with anti-Dystroglycan (DG, green) in w^{1118} control and $Mgat1^{1}$/Df mutant. (B) Representative western blots double-labeled for Fas2 and HRP (left) and DG and VVA lectin (right) in w^{1118} and $Mgat1^{1}$/Df. Alpha tubulin is the loading control. (C) Confocal fluorescence intensity quantification shows no significant (n.s.) change in Fas2 or DG at the NMJ in either homozygous $Mgat1^{1}$ or $Mgat1^{1}$/Df conditions compared with w^{1118}. ANOVA statistical analyses were carried out on a sample size of $n \geq 16$ NMJs for each genotype.

$P<0.001$; Fig. 1C). Anti-HRP recognizes at least 18 protein bands in western blots (Fig. 1D) (Desai et al., 1994). All these N-glycans are lost in *Mgat1* nulls and restored by UH1-Gal4 driven UAS-*Mgat1* (Fig. 1D). The VVA lectin signal is similarly lost in *Mgat1* mutants and rescued with UH1-Gal4 driven UAS-*Mgat1* (w^{1118}: 1.0±0.06; $Mgat1^{1}$: 0.02±0.004, $P<0.001$; $Mgat1^{1}$/Df: 0.04±0.01, $P<0.001$; Fig. 1A,C). By contrast, the endogenous MTG lectin is highly elevated at *Mgat1* null NMJs, as revealed by transgenic MTG tagged with green fluorescent protein (GFP) (Fig. 1E). Quantification of MTG-GFP within FAS2-labeled synaptic domains shows a ~70% increase in nulls compared with controls ($Mgat1^{+9}$ precise excision: 88.53±10.55; $Mgat1^{1}$ null: 149.46±9.52, $P<0.001$). Together, these changes predict strong effects on NMJ synaptogenesis.

FAS2 is the best-characterized HRP-epitope protein, with crucial roles in the development of the *Drosophila* NMJ (Desai et al., 1994; Beumer et al., 2002). Similarly, Dystroglycan (DG) is reportedly the primary substrate for VVA labeling at the NMJ (Haines et al., 2007; Nakamura et al., 2010). Both HRP and VVA labeling are absent at *Mgat1* null NMJs (Fig. 1), allowing analyses of the effects of loss glycosylation on FAS2 and DG expression and synaptic localization (Fig. 2). Specific antibodies against FAS2 and DG show no detectable differences in protein abundance and localization at the NMJ in *Mgat1* nulls compared with controls (Fig. 2A). Western blot analyses likewise show no detectable changes in FAS2 or DG protein stability or expression (Fig. 2B). Quantification of NMJ fluorescence intensities did not show significant changes in *Mgat1* nulls compared with controls for FAS2 (normalized w^{1118}: 1.0±0.04; $Mgat1^{1}$: 1.03±0.05; $Mgat1^{1}$/Df: 0.86±0.08; n.s., not significant; Fig. 2C) or DG (w^{1118}: 1.0±0.02; $Mgat1^{1}$: 1.06±0.01, $Mgat1^{1}$/Df: 1.04±0.04; Fig. 2C). Numerous other lectins used as probes, including WGA, PNA, SBA, ECL and WFA (see Materials and methods), did not show detectable changes in *Mgat1* nulls compared with w^{1118} controls. Quantification of fluorescence intensities revealed no significant differences (data not shown). Together, these results show specific lectin changes at *Mgat1* null NMJs, with loss of HRP and VVA labeling but not other lectin labels, but no changes in the abundance or synaptic localization of prominent HRP- (FAS2) and VVA- (DG) labeled proteins.

Development of NMJ structural overgrowth in the *Mgat1* null condition

Our recent genomic survey of glycosylation genes suggested that glycan mechanisms largely function to restrict morphological growth during *Drosophila* NMJ synaptogenesis (Dani et al., 2012). Synaptic architecture is determined by axonal growth properties, branch formation and the differentiation of synaptic boutons as sites of synaptic vesicle storage for neurotransmitter release (Broadie et al., 2011; Nahm et al., 2013). To assay these structural parameters in *Mgat1* mutants, wandering third instar 6/7 NMJs were labeled with anti-FAS2 and measurements made of NMJ length, branch number (process with at least two boutons) and bouton number (≥1 μm in diameter) in six genotypes: w^{1118} background control, $Mgat1^{+9}$ precise excision control, $Mgat1^{1}$ homozygous and $Mgat1^{1}$/Df null mutants, and muscle 24B-Gal4 and ubiquitous UH1-Gal4 driven UAS-*Mgat1* rescue conditions. Neuronally driven UAS-*Mgat1* resulted in early developmental lethality, and is therefore not included. A summary of these data is shown in Fig. 3.

Null *Mgat1* mutants show a clear increase in NMJ size and structural complexity (Fig. 3A). Quantification of type 1 bouton number shows a highly significant increase in mutants normalized to control, rescued with ubiquitous but not muscle-targeted *Mgat1*, suggesting a neuronal requirement (w^{1118}: 1.0±0.03; $Mgat1^{+9}$: 1.02±0.08; $Mgat1^{1}$: 1.50±0.06, $P<0.001$; $Mgat1^{1}$/Df: 1.58±0.05, $P<0.001$; 24B-Gal4 driven UAS-*Mgat1*: 1.49±0.06; UH1-Gal4 driven UAS-*Mgat1*: 0.97±0.08; Fig. 3B, left). Similarly, quantification of synaptic branch number shows a highly significant increase in *Mgat1* nulls, rescued only with ubiquitous *Mgat1* (w^{1118}: 1.0±0.03; $Mgat1^{+9}$: 0.92±0.08; $Mgat1^{1}$: 1.36±0.06, $P<0.001$; $Mgat1^{1}$/Df: 1.26±0.03, $P<0.001$; UH1-Gal4 driven UAS-*Mgat1*: 0.89±0.06; Fig. 3B, middle). Finally, synaptic growth, quantified as normalized NMJ length, shows a highly significant increase in *Mgat1* mutants, rescued only with ubiquitous *Mgat1* (w^{1118}: 1.0±0.03; $Mgat1^{+9}$: 1.14±0.09; $Mgat1^{1}$: 1.81±0.08, $P<0.001$; $Mgat1^{1}$/Df: 1.53±0.05, $P<0.001$; 24B-Gal4 driven UAS-*Mgat1*: 1.73±0.11, $P<0.001$; UH1-Gal4 driven UAS-*Mgat1*: 0.98±0.05; Fig. 3B, right). Muscle 24B-Gal4 expression of UAS-*Mgat1* did not rescue any structural parameters, suggesting that ubiquitous or at least neuronal *Mgat1* function is required to restore NMJ developmental growth and normal structural synaptogenesis.

Pre- and postsynaptic *Mgat1* roles restrict synaptic functional differentiation

Regulation of *Drosophila* NMJ structural and functional synaptogenesis is often genetically separable, but N-glycans are

Development (2013) doi:10.1242/dev.099192

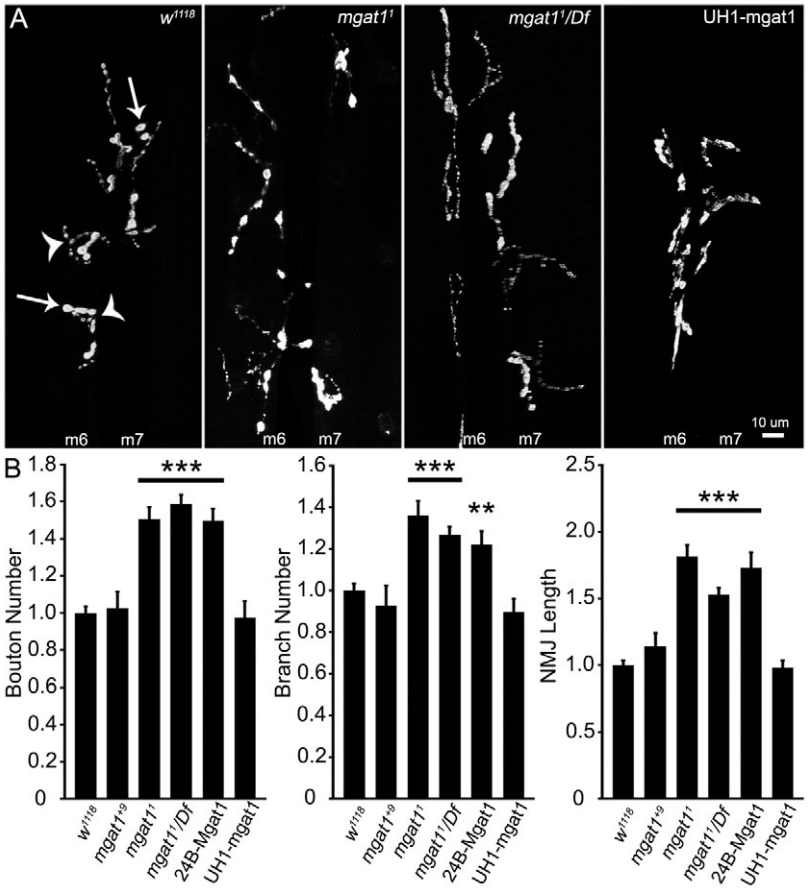

Fig. 3. *Drosophila* NMJ is structurally overgrown in *Mgat1* null mutants. NMJ length, axon branching and synaptic bouton number are increased in *Mgat1* nulls. (A) Representative images of wandering third instar 6/7 NMJ in genetic control (w^{1118}), $Mgat1^{1}$ null, $Mgat1^{1}$/Df(2)BSC430 and UH1-Gal4 driven UAS-*Mgat1* in null background. Representative axon branch points (arrowheads) and boutons (arrows) are illustrated. (B) Quantification of bouton number, branch number and NMJ length normalized to w^{1118} for the $Mgat1^{+9}$ precise excision control, $Mgat1^{1}$ homozygous null, $Mgat1^{1}$/Df and UAS-*Mgat1* driven in muscle (24B-Gal4) or ubiquitously (UH1-Gal4) in the $Mgat1^{1}$/Df background. All three structural parameters are increased in *Mgat1* nulls and fully rescued by ubiquitous UAS-*Mgat1* expression, but not muscle-targeted expression. $^{**}P \leq 0.01$ and $^{***}P \leq 0.001$ (ANOVA) compared with w^{1118}. Sample size is at least eight NMJs from at least four animals from each of the six genotypes shown.

causally implicated in both developmental processes (Broadie et al., 2011; Dani et al., 2012). However, there have been no studies to assess overall N-glycan contributions to functional synaptic differentiation. We therefore next tested functional properties of *Mgat1* null NMJs by measuring synaptic currents using two-electrode voltage-clamp (TEVC) recording. The motor nerve was stimulated with a glass suction electrode at suprathreshold levels to recruit both motoneuron inputs on muscle 6, and the excitatory junction current (EJC) recorded at 0.5 Hz to measure neurotransmission strength. In total, 12 genotypes were assayed: in addition to those described above, including *Mgat1* nulls lacking maternal contribution; ubiquitous, neuron-targeted and muscle-targeted *Mgat1* RNAi; and appropriate controls for transgenic conditions. A summary of these data is shown in Fig. 4.

NMJ functional strength was clearly and consistently increased in all *Mgat1* loss-of-function conditions (Fig. 4A). Null zygotic mutants were comparable to animals lacking both maternal and zygotic expression, showing that a maternal contribution does not mask additional requirements. Mean EJC amplitudes were very significantly elevated in *Mgat1* mutants normalized to genetic control (w^{1118}: 1.0±0.02; $Mgat1^{1}$: 1.45±0.10, $P<0.001$; $Mgat1^{1}$ without maternal contribution: 1.38±0.06, $P<0.001$; $Mgat1^{1}$/Df: 1.40±0.05, $P<0.001$; Fig. 4A,B). Ubiquitous RNAi *Mgat1* knockdown with UH1-Gal4 replicated this phenotype, and the elevated transmission was rescued by ubiquitous expression of UAS-*Mgat1* in $Mgat1^{1}$/Df (w^{1118}: 1.0±0.02; UH1-Gal4/+ control: 0.99±0.04; UH1-Gal4 UAS-RNAi-*Mgat1*: 1.39±0.06, $P<0.001$; UH1-Gal4 UAS-*Mgat1*: 1.07±0.05; Fig. 4C,D). Moreover, postsynaptic *Mgat1* RNAi knockdown also increased EJC amplitude, albeit more moderately, and was rescued with postsynaptic 24B-Gal4 UAS-*Mgat1* in $Mgat1^{1}$/Df (w^{1118}: 1.0±0.02; 24B-Gal4/+ control: 1.04±0.05; 24B-Gal4 UAS-RNAi-*Mgat1*: 1.29±0.06, $P<0.01$; Fig. 4E,D). Finally, presynaptic *Mgat1* RNAi also elevated transmission strength (w^{1118}: 1.0±0.02; *elav*-Gal4/+ control: 0.96±0.05; *elav*-Gal4, UAS-RNAi-*Mgat1*: 1.51±0.11, $P<0.001$; Fig. 4G,H). These results reveal separable pre- and postsynaptic *Mgat1* roles limiting NMJ functional differentiation.

MGAT1 regulates development of synaptic vesicle cycling properties

As loss of *Mgat1* function increases both synaptic morphogenesis and functional differentiation, the next step was to determine whether the overgrown structure simply mediates more transmission, or if structural and functional defects are due to separable *Mgat1* requirements. Synaptic vesicle (SV) cycling with FM1-43 dye measures synaptic function within single boutons, thus allowing a clear separation of structure and function (Long et al., 2010; Nahm et al., 2013). To study SV endocytosis, FM1-43 dye was loaded under endogenous activity conditions over a prolonged period, and in response to acute depolarization with 90 mM K+ saline. To study SV exocytosis, NMJ terminals were depolarized a second time in the absence of FM1-43 to drive dye release. The ratio of loading to unloading provides a measure of SV cycling rate within individual synaptic boutons. A summary of these data is shown in Fig. 5.

Representative images of endogenous activity loading is shown in control and $Mgat1^{1}$/Df NMJs at 1, 10 and 30 minutes in Fig. 5A. Faint dye incorporation was present in boutons (arrows) after 1 minute loading in both genotypes; however, loading occurred significantly faster in control compared with mutant (Fig. 5A,B).

Development (2013) doi:10.1242/dev.099192

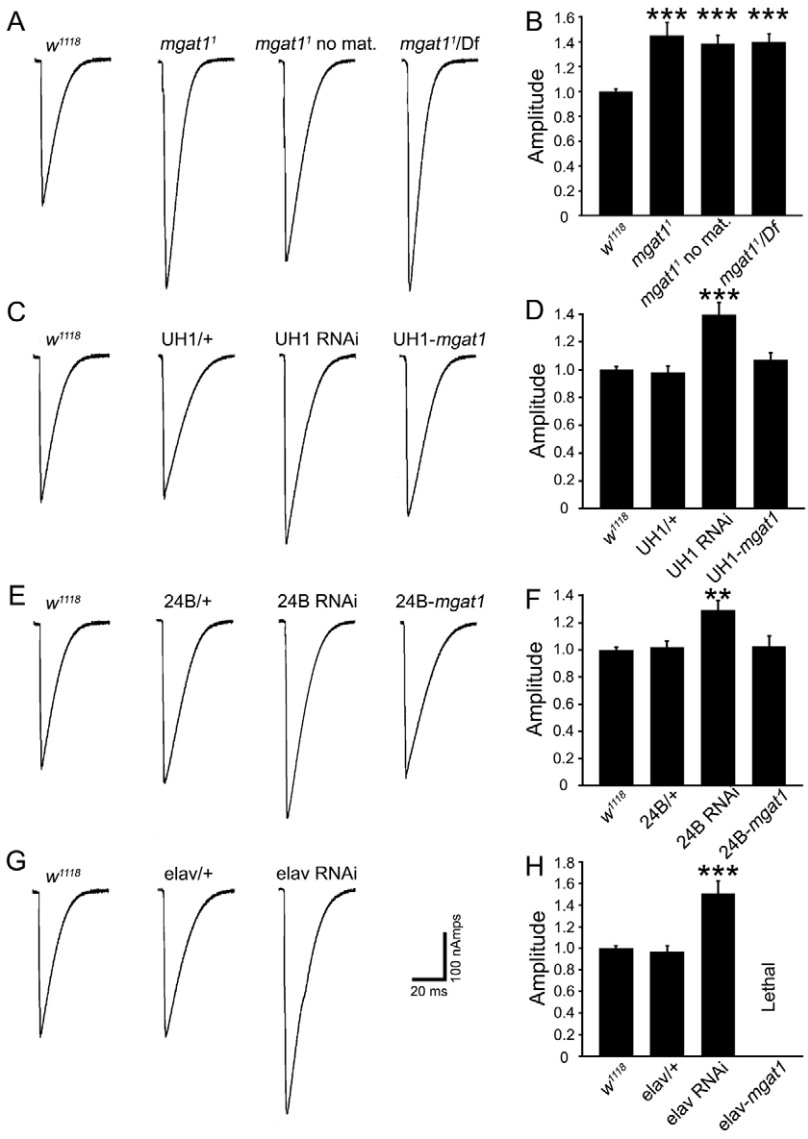

Fig. 4. Strengthened synaptic functional differentiation in *Mgat1* null mutants. Neurotransmission measured using TEVC of stimulation-evoked EJCs at the wandering third instar muscle 6 NMJ. (A) Representative EJC traces recorded in 1.0 mM Ca^{2+} from w^{1118}, *Mgat1*^{1} null, *Mgat1*^{1} without maternal contribution and *Mgat1*^{1}/Df. (B) EJC quantification for all four genotypes normalized to genetic control. Sample size is at least tn animals per genotype. (C) Traces from w^{1118}, UH1/+ control, UH1-GAL4 driven UAS-*Mgat1*-RNAi and UH1-GAL4 driven UAS-*Mgat1* in *Mgat1*^{1}/Df background. Synaptic transmission is elevated by ubiquitous RNAi knockdown and fully restored with reintroduction of ubiqutousUAS-*Mgat1*. (D) EJC quantification for all four genotypes normalized to w^{1118}. Sample size is ≥14 animals per genotype. (E) Traces from w^{1118}, 24B-GAL4/+ control, 24B-GAL4 driven UAS-*Mgat1*-RNAi and 24B-GAL4 driven UAS-*Mgat1* in null background. Transmission elevated by postsynaptic RNAi and rescued with postsynaptic UAS-*Mgat1*. (F) EJC quantification for four genotypes normalized to w^{1118}. Sample size is ≥11 animals per genotype. (G) Traces from w^{1118}, *elav*-GAL4/+ control and *elav*-GAL4 driven UAS-*Mgat1*-RNAi. Transmission is elevated with neuronal RNAi knockdown. (H) EJC quantification normalized to w^{1118}. Sample size is ≥11 animals per genotype. $^{**}P \leq 0.01$ and $^{***}P \leq 0.001$ (ANOVA).

Comparing intensities over time points revealed a significant decrease in *Mgat1* loading [1 minute: 23.1±1.9 (w^{1118}) versus 5.0±0.3 (*Mgat1*), $P<0.0001$; 10 minutes: 79.5±3.5 (w^{1118}) versus 37.3±2.2 (*Mgat1*), $P<0.0001$; 30 minutes: 124.8±12.6 (w^{1118}) versus 74.7±6.6 (*Mgat1*), $P<0.006$; Fig. 5B]. This difference could represent reduced central activity in locomotor pattern generation, reduced SV cycling in the NMJ or elevated dye release compared with uptake. To distinguish these possibilities, FM1-43 dye was loaded (5 minutes) and then partially unloaded (2 minutes) with acute high [K+] depolarization (Fig. 5C). Representative images control and *Mgat1*^{1}/Df NMJs are shown on the left, with higher magnification images of individual boutons shown on the right. Two defects are qualitatively apparent: *Mgat1* nulls incorporate less dye, but release dye faster (Fig. 5C). Quantification of mean fluorescence intensities shows decreased loading in *Mgat1* nulls normalized to control (w^{1118}: 1.0±0.03; *Mgat1*^{1}: 0.83±0.04, $P<0.05$; *Mgat1*^{1}/Df: 0.76±0.04, $P<0.001$; Fig. 5D, left). More strikingly, SV cycling rate (unloaded/loaded fluorescence intensity) is increased in *Mgat1* nulls compared with control (w^{1118}: 1.0±0.05; *Mgat1*^{1}: 0.46±0.05, $P<0.001$; *Mgat1*^{1}/Df: 0.37±0.03, $P<0.001$; Fig. 5D, right). Thus, *Mgat1* mutants exhibit altered SV cycling within individual boutons, independent of the increased bouton number, with a strong increase in cycling rate in response to acute depolarization.

Selective loss of pre-and postsynaptic components in *Mgat1* null mutants

Functional differentiation of the NMJ requires recruitment and organization of presynaptic SV cycle proteins and AZ release sites, and postsynaptic glutamate receptors (GluRs; Featherstone et al., 2005; Long et al., 2008; Richmond and Broadie, 2002). N-glycosylation may be important for localization and maintenance of these key proteins during synaptogenesis, hypothesized to be dependent on MGAT1 function (Dani et al., 2012; Kwon and Chapman, 2012). We therefore next conducted a thorough confocal microscopy expression survey of synaptic proteins in the *Mgat1* null condition to test for changes in presynaptic and postsynaptic composition. Most proteins were unchanged in *Mgat1* mutants, and only a few molecular changes were identified. A summary of these results is shown in Fig. 6.

Postsynaptic GluRs are believed to form tetramers composed of three essential subunits (GLURIIC-E) and a single variable subunit (GLURIIA or B) generating two distinct GluR functional classes

Development (2013) doi:10.1242/dev.099192

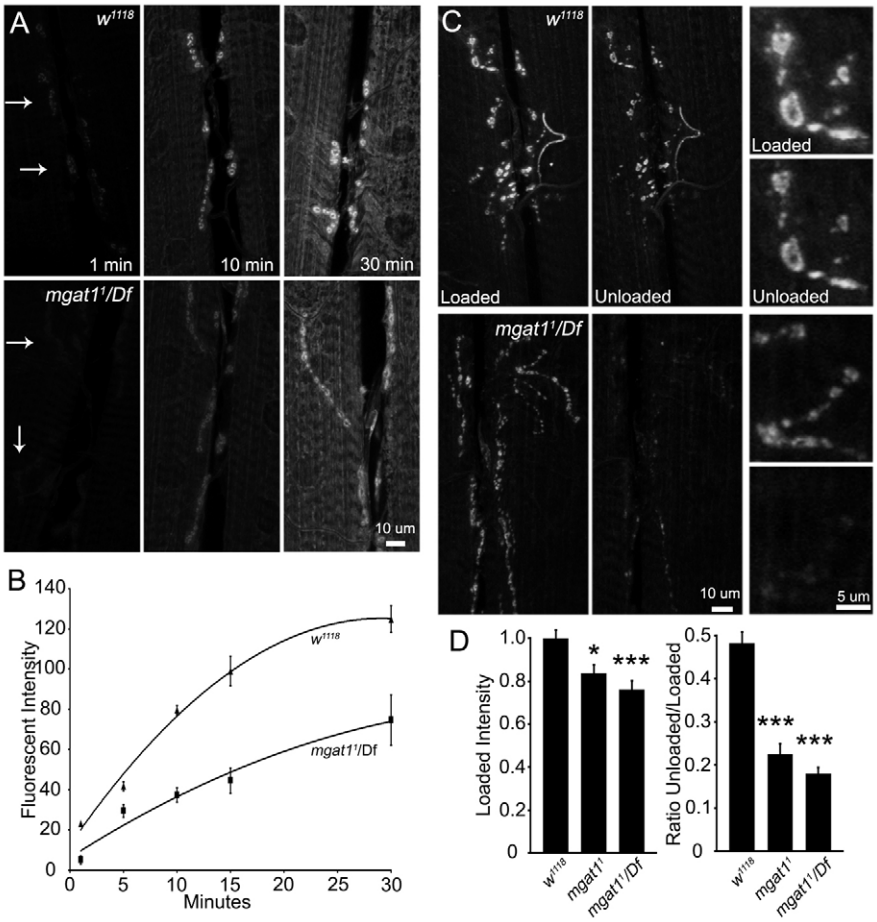

Fig. 5. Altered NMJ synaptic vesicle cycling in the *Mgat1* null mutants. Assays of synaptic vesicle (SV) loading and cycling rates with FM1-43 dye imaging at the wandering third instar 6/7 NMJ. (A) Representative images of FM1-43 loading during endogenous activity at 1, 10 and 30 minutes. Top panels show w^{1118} control and bottom panels show $Mgat1^{1}$/Df. Arrows indicate boutons faintly loaded at 1 minute. (B) Fluorescence intensity plotted at 1, 5, 10, 15 and 30 minutes of endogenous activity; at least nine animals per genotype used for each time point. (C) Representative NMJ images after FM1-43 loading with 90mM K^+ for 5 minutes and unloading for 2 minutes. Top panels show w^{1118} and bottom panels show $Mgat1^{1}$/Df, with increased SV turnover indicated by reduced intensity after unloading. Right panels show high magnification images of loaded/unloaded boutons. (D) Quantification of loading and ratio of unloaded/loaded fluorescence intensities for w^{1118}, $Mgat1^{1}$ homozygous null and $Mgat1^{1}$/Df. *P≤0.05, **P≤0.01 and ***P≤0.001 (ANOVA) compared with genetic control w^{1118}. Sample size is ≥18 NMJs for each genotype.

(Featherstone et al., 2005; Qin et al., 2005). To assay these receptor classes, we probed control and *Mgat1* null NMJs with antibodies specific for GLURIIA, B and C subunits. There was no detectable change in the overall expression of total GluRs (labeled with the essential GLURIIC) or the GLURIIA-class receptors in the *Mgat1* null condition (data not shown). By contrast, there was a clear and obvious decrease in GLURIIB-class receptors in *Mgat1* nulls, both at low level magnification of the entire NMJ and in higher resolution images of individual synaptic boutons (Fig. 6A). Quantitative measures of fluorescence intensity show a highly significant decrease in GLURIIB labeling in $Mgat1^{1}$/Df normalized to the genetic control (w^{1118}: 1.0±0.09; $Mgat1^{1}$/Df: 0.73±0.04, P<0.01; Fig. 6D, left). This selective loss of GLURIIB shows that this one receptor class alone appears dependent on MGAT1 function.

The presynaptic apparatus includes key AZ protein Bruchpilot (BRP), V/T-SNARES of the core SNARE complex, and a host of SV associated and integral proteins regulating the SV cycle (Chapman, 2002; Hallermann et al., 2010). We assayed a wide range of these presynaptic proteins for changes in *Mgat1* null mutants, and found that all did not detectably change, with only a single exception. The BRP punctae marking AZs were clearly decreased in *Mgat1* mutants, both in whole NMJs and in high magnification images of synaptic boutons (Fig. 6B). Quantification of BRP labeling intensities showed a significant decrease in $Mgat1^{1}$/Df normalized to control (w^{1118}: 1.0±0.07; $Mgat1^{1}$/Df: 0.80±0.05, P<0.05; Fig. 6D). By contrast, other presynaptic components [e.g. Synaptotagmin, Cysteine string protein (CSP), Synaptogyrin (GYR)] were not detectably altered in *Mgat1* nulls (data not shown). As exemplars of these negative data, we show vesicular glutamate transporter (VGLUT) and V-SNARE Synaptobrevin (Fig. 6D). The selective loss of just BRP shows a focused presynaptic requirement for MGAT1 function.

Multiple trans-synaptic signaling pathways altered in *Mgat1* null mutants

Active zone (i.e. BRP) and class-specific GluR (i.e. GLURIIB) recruitment are both dependent on tightly regulated trans-synaptic signaling between pre- and postsynaptic cells during synaptogenesis (Dani et al., 2012; Marqués, 2005; Rohrbough et al., 2013). Moreover, both trans-synaptic signaling pathway components and the synaptomatrix they traverse are highly glycosylated, and it is known that glycan mechanisms play key roles in the regulation of this developmental communication (Rohrbough and Broadie, 2010; Rohrbough et al., 2013). We therefore hypothesized that *Mgat1* mutants would manifest defects in bidirectional trans-synaptic signals. To test this idea, we assayed signaling ligands for three well-characterized trans-synaptic pathways: (1) anterograde Wnt Wingless (WG); (2) retrograde BMP Glass bottom boat (GBB); and (3) newly defined ligand Jelly belly (JEB). Representative NMJ images and the compiled quantification for these studies are shown in Fig. 7.

Well-characterized antibodies for all three signaling ligands were used to label wandering third instar NMJs, comparing fluorescence intensities within the synaptic domain (dotted white outlines) in $Mgat1^{1}$/Df null normalized to the w^{1118} genetic control (Fig. 7). The WG signal was obviously increased in mutants (Fig. 7A, middle), and quantification of fluorescence intensity confirmed a significant elevation (w^{1118}: 1.0±0.10; $Mgat1^{1}$/Df: 1.56±0.16, P<0.001; Fig. 7A,

Development (2013) doi:10.1242/dev.099192

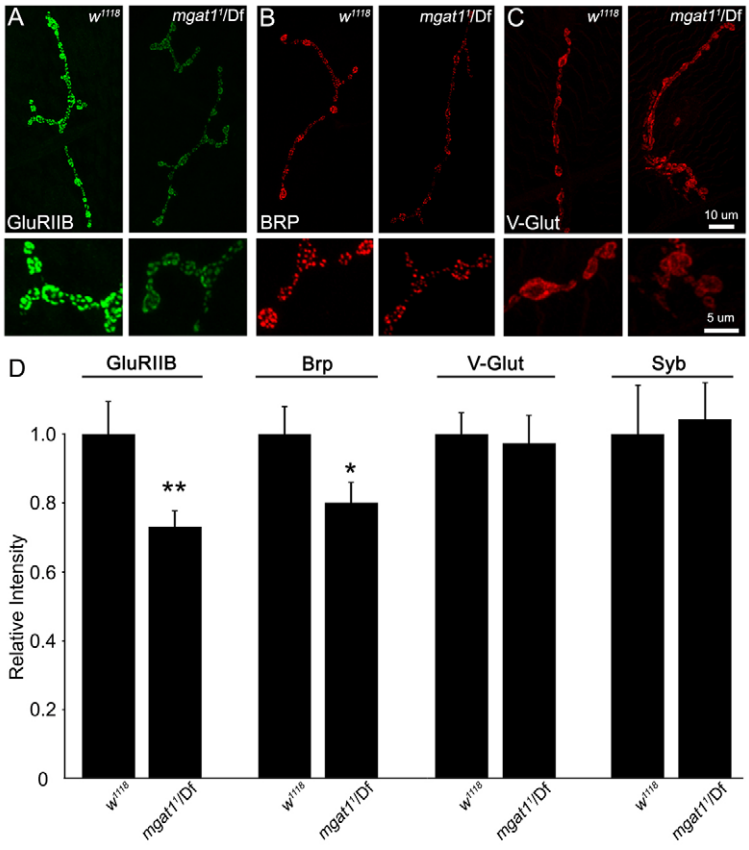

Fig. 6. Pre- and postsynaptic component recruitment reduced at *Mgat1* NMJs. Null *Mgat1* mutants show decreased postsynaptic glutamate receptor type IIB (GLURIIB) and presynaptic active zone Bruchpilot (BRP), but are unchanged for multiple other synaptic components. (A-C) Representative NMJ images for GLURIIB (A, green), BRP (B, red) and the vesicular glutamate transporter (VGLUT; C, red) in genetic control w^{1118} and $Mgat1^{1}$/Df mutants. High-magnification images of synaptic boutons shown below. (D) Quantification of fluorescence intensities for GLURIIB ($n \geq 28$), BRP ($n \geq 38$), VGLUT ($n \geq 12$) and Synaptobrevin (SYB; $n \geq 16$) normalized to w^{1118}. VGLUT and SYB exhibit no change, indicating similar synaptic vesicle related density in control and mutant. *$P \leq 0.05$, **$P \leq 0.01$ and ***$P \leq 0.001$ (Student's *t*-test) for each pairwise comparison.

right). By contrast, the GBB signal was clearly reduced and poorly localized to the synaptic domain in mutants (Fig. 7B, middle), and likewise significantly decreased in quantified intensity (w^{1118}: 1.0±0.08; $Mgat1^{1}$/Df: 0.55±0.08, $P<0.001$; Fig. 7B, right). The third signal JEB was similarly decreased in $Mgat1^{1}$/Df compared with control (w^{1118}: 1.0±0.07; $Mgat1^{1}$/Df: 0.63±0.07 $P<0.01$; Fig. 7C). These results reveal a differential MGAT1 role in modulating trans-synaptic signaling, with increased abundance of WG ligand and decreases in both GBB and JEB ligands. A primary role of trans-synaptic signaling is to recruit synaptic scaffolds, which in turn bind synaptic proteins to seed the process of synaptogenesis.

Loss of key synaptic scaffolds driving synaptogenesis in *Mgat1* null mutants

Discs large 1 (DLG1) is a particularly well-characterized synaptic scaffold at the *Drosophila* NMJ, which is modulated downstream of WG, GBB and JEB trans-synaptic signaling and, in turn, drives the appropriate recruitment of synaptic proteins including cell adhesion molecules, ion channels and GLURIIB-containing receptors (Chen and Featherstone, 2005; Marqués, 2005; Marrus et al., 2004). In addition, we have just recently defined Lethal (2) giant larvae [L(2)GL] as another key synaptic scaffold, which presynaptically facilitates the assembly of BRP-containing active zones to regulate SV cycling, and postsynaptically regulates GluR subunit composition (Staples and Broadie, 2013). We hypothesized that, downstream of MGAT1-dependent changes in trans-synaptic signaling, defects in recruiting these synaptic scaffolds could explain changes in pre/postsynaptic molecular composition. To test this idea, we imaged DLG1 and L(2)GL scaffolds at the wandering third instar NMJ, comparing *Mgat1* nulls to genetic controls. A summary of these data is shown in Fig. 8.

The DLG1 scaffold is expressed in both pre- and postsynaptic compartments, but is most apparent in the subsynaptic reticulum (SSR) overlapping with postsynaptic glutamate receptors (Fig. 8A). DLG1 levels are clearly and strongly decreased in *Mgat1* null mutants compared with controls. When intensity levels were quantified, there was a very significant decrease in mutants normalized to genetic control (w^{1118}: 1.0±0.08; $Mgat1^{1}$: 0.66±0.06, $P<0.01$; Fig. 8C, top). Similarly, the L(2)GL scaffold is present in the FAS2-labeled NMJ terminals in both presynaptic boutons and the postsynaptic domain, with clearly higher levels of expression in genetic control compared with the *Mgat1* null condition (Fig. 8B). Quantification of fluorescence intensity shows a highly significant decrease in L(2)GL (w^{1118}: 1.0±0.07; $Mgat1^{1}$: 0.50±0.06, $P<0.001$; Fig. 8C, bottom). L(2)GL and DLG1 scaffolds are both known to regulate active zone and glutamate receptor composition, so changes in their abundance and localization are likely to be causal in MGAT1-dependent changes in NMJ synaptogenesis.

DISCUSSION

We began with the hypothesis that disruption of synaptomatrix N-glycosylation would alter trans-synaptic signaling underlying NMJ synaptogenesis (Dani and Broadie, 2012). MGAT1 loss transforms the synaptomatrix glycan environment. Complete absence of the HRP epitope, α1-3-fucosylated N-glycans, is expected to require MGAT1 activity: key HRP epitope synaptic proteins include fasciclins, Neurotactin and Neuroglian, among others (Desai et al., 1994; Paschinger et al., 2009). We show that HRP epitope modification of the key synaptogenic regulator Fasciclin 2 is not required for stabilization or localization, suggesting a role in protein function. However, complete loss of VVA lectin synaptomatrix labeling is surprising because the epitope is a terminal β-GalNAc

Development (2013) doi:10.1242/dev.099192

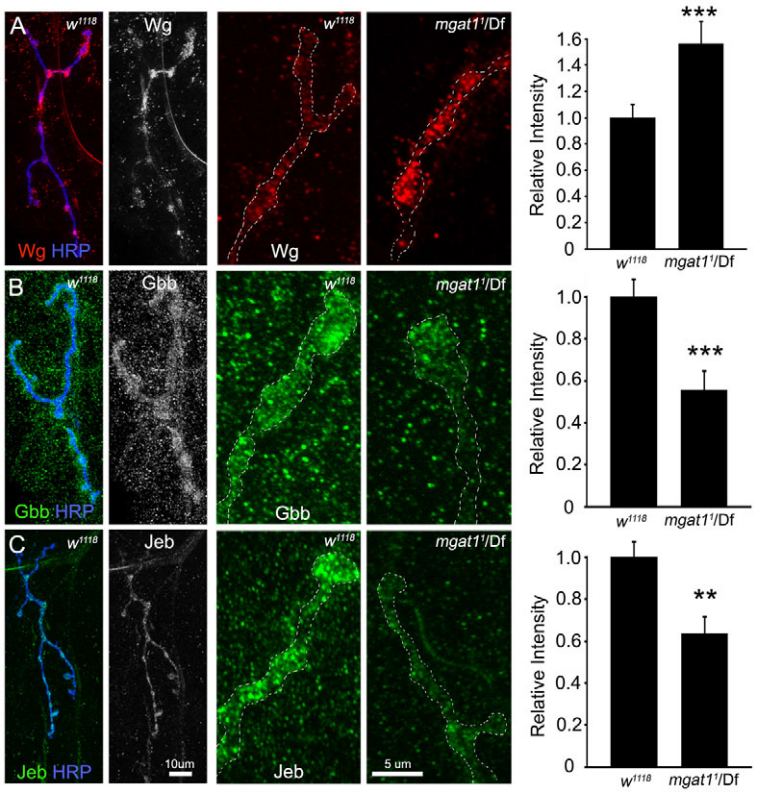

Fig. 7. Multiple trans-synaptic signaling pathways altered in *Mgat1* null mutant. Assays of three well-characterized NMJ trans-synaptic signals: Wingless (WG), Glass bottom boat (GBB) and Jelly belly (JEB). (A) Representative NMJ images of WG (red) double-labeled with HRP (blue), and shown alone (WG, white). High-magnification bouton comparison of genetic control (w^{1118}) and $Mgat1^{1}$/Df. Right: Quantification of relative fluorescence intensity reveals increased WG in mutant. (B) Representative images of GBB (green) double-labeled with HRP (blue), and shown alone (GBB, white). High-magnification bouton comparison of w^{1118} and $Mgat1^{1}$/Df. Right: Quantification shows decreased GBB in mutant. (C) Representative NMJ images of JEB (green) double-labeled with HRP (blue), and shown alone (JEB, white). High-magnification bouton comparison of w^{1118} and $Mgat1^{1}$/Df. Right: Quantification shows decreased JEB in mutant. Fluorescence intensities measured within the NMJ domain (white dotted line), normalized to genetic control w^{1118}. $^{**}P \leq 0.01$ and $^{***}P \leq 0.001$ (Student's *t*-test) for pairwise comparisons. The sample size is $n \geq 18$ NMJs for each label and each genotype.

(Martin, 2003). This result suggests that the N-glycan LacdiNAc is enriched at the NMJ, and that the terminal GalNAc expected on O-glycans/glycosphingolipids may be present on N-glycans in this synaptic context. Importantly, VVA labels Dystroglycan and loss of Dystroglycan glycosylation blocks extracellular ligand binding and complex formation in *Drosophila* (Haines et al., 2007; Nakamura et al., 2010), and causes muscular dystrophies in humans (Ervasti et al., 1997; Muntoni et al., 2008; Tran et al., 2012). This study shows that VVA-recognized Dystroglycan glycosylation is not required for protein stabilization or synaptic localization, but did not test functionality or complex formation, which probably requires MGAT1-dependent modification. Conversely, the secreted endogenous lectin MTG is highly elevated in *Mgat1* null synaptomatrix, probably owing to attempted compensation for complex and hybrid N-glycan losses that serve as MTG binding sites. MTG binds GlcNAc in a calcium-dependent manner and pulls down a number of HRP-epitope proteins by immunoprecipitation (Rushton et al., 2012), although the specific proteins have not been identified. It will be of interest to perform immunoprecipitation on *Mgat1* samples to identify changes in HRP bands. Importantly, MTG is crucial for synaptomatrix glycan patterning and functional synaptic development (Rohrbough et al., 2007). MTG regulates VVA synaptomatrix labeling (Rushton et al., 2009), suggesting a mechanistic link between the VVA and MTG changes in *Mgat1* mutants. The MTG elevation observed in *Mgat1* nulls provides a plausible causative mechanism for strengthened functional differentiation (Rohrbough and Broadie, 2010; Rushton et al., 2012).

Consistent with our recent glycosylation gene screen findings (Dani et al., 2012), *Mgat1* nulls exhibit increased synaptic growth and structural overelaboration. Therefore, complex and hybrid N-glycans overall provide a brake on synaptic morphogenesis, although individual N-glycans may provide positive regulation. Likely players include MGAT1-dependent HRP-epitope proteins (e.g. fasciclins, Neurotactin, Neuroglian), and position-specific (PS) integrin receptors and their ligands, all of which are heavily glycosylated and have well-characterized roles regulating synaptic architecture (Beumer et al., 1999; Rushton et al., 2009; Beck et al., 2012; Enneking et al., 2013). An alternative hypothesis is that *Mgat1* phenotypes may result from the presence of high-mannose glycans on sites normally carrying complex/hybrid structures (Schachter, 2010), suggesting possible gain of function rather than loss of function of specific N-glycan classes. NMJ branch and bouton number play roles in determining functional strength (Thomas and Sigrist, 2012), although active zones and GluRs are also regulated independently (DiAntonio, 2006). Thus, the increased functional strength could be caused by increased structure at *Mgat1* null NMJs. However, muscle-targeted UAS-*Mgat1* rescues otherwise *Mgat1* null function, but has no effect on structural defects, demonstrating that these two roles are separable. Presynaptic *Mgat1* RNAi also causes strong functional defects, showing there is additionally a presynaptic requirement in functional differentiation. Neuron-targeted *Mgat1* causes lethality, indicating that MGAT1 levels must be tightly regulated, but preventing independent assessment of *Mgat1* presynaptic rescue of synaptogenesis defects.

Presynaptic glutamate release and postsynaptic glutamate receptor responses drive synapse function. Using lipophilic dye to visualize SV cycling, we found *Mgat1* null mutants endogenously cycle less than controls, but have greater cycling capacity upon depolarizing stimulation. The endogenous cycling defect is consistent with the sluggish locomotion of *Mgat1* mutants (Sarkar et al., 2006), whereas the elevated stimulation-evoked cycling is consistent with electrophysiological measures of neurotransmission. Similarly, mutation of dPOMT1, which glycosylates VVA-labeled Dystroglycan, decreases SV release probability (Wairkar et al., 2008), although dPOMT1 adds mannose not GalNAc. Null *Mgat1*

Development (2013) doi:10.1242/dev.099192

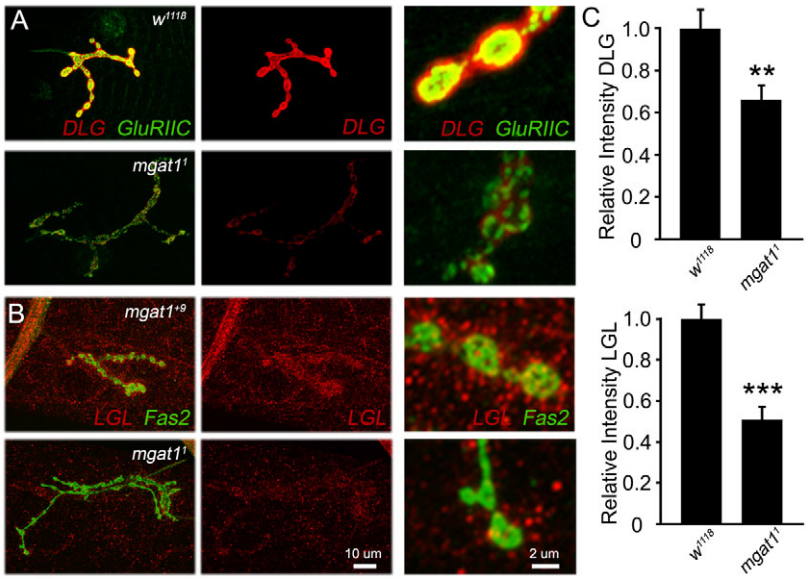

Fig. 8. Synaptic scaffolds DLG1 and L(2)GL reduced in the *Mgat1* null mutants. Imaging of DLG1 and L(2)GL synaptic scaffolds at the wandering third instar NMJ. (A) Representative images of DLG1 (red) co-labeled with glutamate receptor type IIC (GLURIIC, green), with higher magnification boutons in side panels. (B) Representative images of L(2)GL (red) co-labeled with Fas2 (green), with high-magnification boutons in side panels. (C) Quantification of DLG1 fluorescence intensity (top: $Mgat1^{1}$, n=15; w^{1118}, n=22) and L(2)GL fluorescence intensity (bottom: $Mgat1^{1}$, n=12; w^{1118}, n=12). **P≤0.01 and ***P≤0.001 (Student's t-test) for pairwise comparisons.

mutants display no change in SV cycle components (e.g. Synaptobrevin, Synaptotagmin, Synaptogyrin, etc.), but exhibit reduced expression of the key active zone component Bruchpilot (Wagh et al., 2006; Kittel et al., 2006). Other examples of presynaptic glycosylation requirements include the *Drosophila* Fuseless (FUSL) glycan transporter, which is critical for Cacophony (CAC) voltage-gated calcium channel recruitment to active zones (Long et al., 2008), and the mammalian GalNAc transferase (GALGT2), whose overexpression causes decreased active zone assembly (Martin, 2003). Postsynaptically, *Mgat1* nulls show specific loss of GLURIIB-containing receptors. Similarly, dPOMT1 mutants exhibit specific GLURIIB loss (Wairkar et al., 2008), although *dystroglycan* nulls display GLURIIA loss (Bogdanik et al., 2008). Selective GLURIIB loss in *Mgat1* nulls may drive increased neurotransmission owing to channel kinetics differences in GLURIIA versus GLURIIB receptors (DiAntonio et al., 1999).

Bidirectional trans-synaptic signaling regulates NMJ structure, function and pre/postsynaptic composition (Dani et al., 2012; Enneking et al., 2013; Müller and Davis, 2012). This intercellular signaling requires ligand passage through, and containment within, the heavily glycosylated synaptomatrix (Dani and Broadie, 2012; Martin, 2003), which is strongly compromised in *Mgat1* mutants. In testing three well-characterized signaling pathways, we found that WG accumulates, whereas both GBB and JEB are reduced in the *Mgat1* null synaptomatrix. WG has two N-glycosylation sites, but these do not regulate ligand expression (Tang et al., 2012), suggesting WG build-up occurs owing to lost synaptomatrix N-glycosylation. Importantly, WG overexpression increases NMJ bouton formation similarly to the phenotype of *Mgat1* nulls (Ataman et al., 2008; Korkut et al., 2009), suggesting a possible causal mechanism. GBB is predicted to be N-glycosylated at four sites, but putative glycosylation roles have not yet been tested. Importantly, GBB loss impairs presynaptic active zone development similarly to *Mgat1* nulls (McCabe et al., 2003; Nahm et al., 2010), suggesting a separable causal mechanism. JEB is not predicted to be N-glycosylated, indicating that JEB loss is caused by lost synaptomatrix N-glycosylation. Importantly, we have just recently shown that loss of JEB signaling increases functional synaptic differentiation similarly to *Mgat1* nulls (Rohrbough et al., 2013). In addition, *jeb* mutants exhibit strongly suppressed NMJ endogenous activity, similarly to the reduced endogenous SV cycling in *Mgat1* nulls (Rohrbough and Broadie, 2010). Moreover, the MTG lectin negatively regulates JEB accumulation in NMJ synaptomatrix (Rohrbough and Broadie, 2010), consistent with elevated MTG causing JEB downregulation in *Mgat1* nulls.

Trans-synaptic signaling drives recruitment of scaffolds that, in turn, recruit pre- and postsynaptic molecular components (Ataman et al., 2006; Koles et al., 2012). Specifically, DLG1 and L(2)GL scaffolds regulate the distribution and density of both active zone components (e.g. BRP) and postsynaptic GluRs (Chen and Featherstone, 2005; Staples and Broadie, 2013), and both of these scaffolds are reduced at *Mgat1* null NMJs. Importantly, *dlg1* mutants display selective loss of GLURIIB, with GLURIIA unchanged, similar to *Mgat1* nulls (Chen and Featherstone, 2005), suggesting a causal mechanism. Moreover, *l(2)gl* mutants display both a selective GLURIIB impairment as well as reduction of BRP aggregation in active zones, similarly to *Mgat1* nulls (Staples and Broadie, 2013), suggesting a separable involvement for this synaptic scaffold. DLG1 and L(2)GL are known to interact in other developmental contexts (Humbert et al., 2008), indicating a likely interaction at the developing synapse. Although synaptic ultrastructure has not been examined in *l(2)gl* mutants, *dlg1* mutants exhibit impaired NMJ development, including a deformed SSR (Lahey et al., 1994). These synaptogenesis requirements predict similar ultrastructural defects in *Mgat1* mutants, albeit presumably due to the combined loss of both DLG1 and L(2)GL scaffolds. Our future work will focus on electron microscopy analyses to probe N-glycosylation mechanisms of synaptic development.

MATERIALS AND METHODS

Drosophila genetics

All genotypes were made in the w^{1118} background, with w^{1118} used as genetic control. Df(2R)BSC430 removing *Mgat1* was obtained from the Bloomington *Drosophila* Stock Center (Indiana University). Imprecise excision $Mgat1^{1}$ and precise excision $Mgat1^{+9}$ lines have been characterized (Sarkar et al., 2006). Transgenic studies were done with the pan-neural *elav*-Gal4, muscle 24B-Gal4 and ubiquitous UH1-Gal4 driver lines (Brand and Perrimon, 1993; Lin and Goodman, 1994; Rohrbough et al., 2007) crossed to UAS-*Mgat1* (Sarkar et al., 2010) or UAS-RNAi-*Mgat1* lines obtained from the Vienna *Drosophila* RNAi Center (VDRC). The Mind the gap (MTG) cDNA fused to GFP coding sequence (UAS-MTG:GFP; Rushton et

al., 2009) was placed into *w*; *Mgat1*^{1}/Cyo-GFP to express MTG:GFP in the null background.

Immunocytochemistry

Studies were performed as described previously (Rushton et al., 2012; Dani et al., 2012). Briefly, wandering third instars were dissected in physiological saline consisting of 128 mM NaCl, 2 mM KCl, 4 mM $MgCl_2$, 0.2 mM $CaCl_2$, 70 mM sucrose, 5 mM trehalose and 5 mM 2-[4-(2-hydroxyethyl)piperazin-1-yl]ethanesulfonic acid (HEPES) (pH 7.1). Preparations were fixed in ice-cold methanol for 5 minutes (GLURIIA) or 4% paraformaldehyde for 10 minutes at room temperature (RT; all other labels). Preparations were then either processed with detergent [phosphate-buffered saline (PBS) + 1% bovine serum albumin (BSA) + 0.2% Triton X-100] for cell-permeabilized studies, or detergent-free (PBS with 1% BSA) conditions for non-permeabilized studies. Primary antibodies used included: rabbit anti-HRP (1:200, Sigma); mouse anti-Fasciclin 2 [FAS2, 1:10, 1D4, Developmental Studies Hybridoma Bank (DSHB), University of Iowa]; rabbit anti-DG (1:1000, gift from Wu Deng, Department of Biological Sciences, The Florida State University); mouse anti-glutamate receptor IIA [GLURIIA, 1:100, 8B4D2(MH2B), DSHB], rabbit anti-GLURIIB (1:1000) (Marrus et al., 2004), and rabbit anti-GLURIIC (1:500) (Marrus et al., 2004); mouse anti-BRP (1:100, NC82, DSHB); rabbit anti-vesicular glutamate transporter (VGLUT, 1:10,000) (Daniels et al., 2004); rabbit anti-SYB (1:500) (Littleton et al., 1993); mouse anti-Cysteine string protein (CSP, 1:250) (Zinsmaier et al., 1990); rabbit anti-Synaptogyrin (GYR, 1:500) (Stevens et al., 2012); mouse anti-Wingless (WG, 1:2, 4D4, DSHB); rabbit anti-GBB (1:100) (Dani et al., 2012), guinea pig anti-JEB (1:2000) (Lee et al., 2003); mouse anti-DLG (1:200, DLG1, DSHB); rabbit anti-L(2)GL (1:300) (Ohshiro et al., 2000). Lectins used included: *Vicia villosa* agglutinin (VVA-Tritc, 1:200, R-4601-2, E.Y. Laboratories); and wheat germ agglutinin (WGA, 1:200, B-1025, Vector Laboratories), peanut agglutinin (PNA, 1:250, B-1075, Vector Laboratories), soybean agglutinin (SBA, 1:200, B-1015, Vector Laboratories), *Erythrina cristagalli* lectin (ECL, 1:250, B-1145, Vector Laboratories) and *Wisteria floribunda* lectin (WFA, 1:250, B-1355, Vector Laboratories), all from Vector Laboratories. Secondary Alexa fluorophore antibodies (Invitrogen) used included: goat anti-mouse 488 and 568 (1:250), goat anti-rabbit 488/568 (1:250), goat anti-guinea pig 488/568 (1:250) and streptavidin 488 (1:250). Primary antibodies and lectins were incubated at 4°C overnight; secondary antibodies were incubated at RT for 2 hours. Dissections were mounted in Fluoromount-G (Electron Microscopy Sciences). *Z*-stacks were taken with a Zeiss LSM 510 META laser-scanning confocal using 40× or 63× Plan Apo oil immersion objectives. Optical sections were done starting immediately above and ending immediately below the NMJ. Stacks were projected on the *z*-axis, with NMJ signals highlighted and average intensity for each recorded. Intensities were quantified using ImageJ (Abramoff et al., 2004).

Western blotting

Dissected wandering third instar ventral nerve cords (6) were homogenized in buffer [67 mM NaCl, 2 M urea, 1.3% sodium dodecyl sulfate (SDS), 1 mM EDTA, Tris pH 8] and centrifuged for 30 minutes at 16,000 ***g***. Soluble fractions with 1× NuPage sample buffer (Invitrogen) and 5% 2-mercaptoethanol were boiled for 10 minutes. Samples were loaded onto 4-12% Bis-Tris SDS gels (Invitrogen), electrophoresed at 200 V for 90 minutes in 1× MES buffer and transferred to nitrocellulose membranes (Biorad) in 1× NuPage transfer buffer with 300 mA for 1 hour at 4°C. Membranes were blocked in 2% BSA (Sigma) in Tris-buffered saline + Tween 20 (TBST; 10 mM Tris pH 8, 150 mM NaCl, 0.05% Tween 20) for 1 hour at RT. Rabbit anti-HRP (Sigma) (1:1000) or biotinylated VVA (EY labs) (1:1000) were diluted in blocking buffer and incubated for 1 hour at RT and washed for 5 minutes in TBST (six times). Mouse anti-tubulin (Sigma) (1:5000), rabbit anti-DG (1:1000) or mouse anti-FAS2 (34B3C2) (1:100) were diluted in blocking buffer and incubated overnight at 4°C. Preparations were washed for 5 minutes with TBST (six times), and streptavidin-800 (Rockland) (1:10,000), goat anti-mouse 680 (Invitrogen) (1:10,000) or goat anti-rabbit 800 (Rockland) (1:10,000) were incubated for 1 hour at RT. Blots were washed for 5 minutes in TBST (six times) and then imaged using an Odyssey Infrared Imaging System.

Electrophysiology

TEVC electrophysiology was performed as previously reported (Rohrbough and Broadie, 2002). Briefly, staged larvae were glued with 3M Vetbond tissue adhesive (World Precision Instruments) to sylgard-coated glass coverslips, cut longitudinally along the dorsal midline, internal organs removed and sides glued down for neuromusculature access. Peripheral nerves were cut near the ventral nerve cord (VNC). Dissections and recordings were performed at 18°C in saline consisting of 128 mM NaCl, 2 mM KCl, 4 mM $MgCl_2$, 1 mM $CaCl_2$, 70 mM sucrose, 5 mM trehalose and 5 mM HEPES (pH 7.1). Preparations were imaged using a Zeiss Axioskop microscope with 40× water immersion objective. A fire-polished glass suction electrode was used for evoked nerve stimulation with a 0.5-msecond supratheshold stimulus at 0.2 Hz from a Grass S88 stimulator (Rohrbough and Broadie, 2010). Muscle 6 in abdominal segments 2/3 was impaled with two microelectrodes of ~15 MΩ resistance filled with 3 M KCl. The muscle was clamped at −60 mV using an Axoclamp-2B amplifier. EJC records were filtered at 2 kHz. To quantify EJC amplitudes, ten consecutive traces were averaged and the peak of the averaged trace recorded. Clampex software was used for all data acquisition, Clampfit software was used for all data analysis, and GraphPad InStat 3 software was used for statistical tests.

FM1-43 dye imaging

Synaptic vesicle cycling was imaged using lipophilic dye FM1-43, as previously reported (Long et al., 2010; Nahm et al., 2013). Briefly, for endogenous labeling, dissected preparations were incubated in physiological saline (1.0 mM Ca^{2+}) plus 10 μM FM1-43 (Invitrogen). To stop loading at staged intervals, the saline was replaced several times in quick succession with Ca^{2+}-free saline lacking FM1-43. For evoked depolarization dye loading, preparations were stimulated with 90 mM K^{+} plus 10 μM FM1-43 for 5 minutes. After imaging, preparations were unloaded with the same depolarizing stimulation without FM1-43 for 2 minutes. *Z*-stacks were taken with a Zeiss LSM 510 META laser-scanning confocal microscope using a 63× water immersion objective. Fifteen slices were acquired and stacks projected in ImageJ. To quantify loaded/unloaded fluorescence intensities, five individual boutons per NMJ were outlined and average intensity measured in ImageJ, with muscle background intensities subtracted.

Statistics

All statistics were performed using GraphPad InStat3 software. ANOVA tests were used for all data sets of at least three comparisons. Student's *t*-test was used for pairwise comparisons.

Acknowledgements

We thankfully acknowledge the Bloomington *Drosophila* Stock Center (Indiana University) and the Developmental Studies Hybridoma Bank (University of Iowa) for genetic lines and antibodies, respectively. We are most grateful to Gabrielle Boulianne (University of Toronto, Canada) for *Mgat1* alleles; and to Wu-Min Deng (Florida State University) for anti-DG, Aaron DiAntonio (Washington University School of Medicine) for anti-GLURIIB/C, Ruth Palmer (Umea Institute, Sweden) for anti-JEB, and Daniela Zarnescu (University of Arizona) for anti-L(2)GL antibodies.

Competing interests

The authors declare no competing financial interests.

Author contributions

W.P. performed and analyzed most of the experiments. M.L.D. ran all western blots and related quantification in Figs 1 and 2. E.R. imaged MTG in Fig. 1E. W.P. and K.B. designed experiments and wrote the manuscript.

Funding

This work was entirely supported by the National Institutes of Health [grant RO1 MH096832 to K.B.]. Deposited in PMC for release after 12 months.

References

Abramoff, M. D., Magalhaes, P. J. and Ram, S. J. (2004). Image processing with ImageJ. *Biophotonics International* **11**, 36-42.

Ataman, B., Ashley, J., Gorczyca, D., Gorczyca, M., Mathew, D., Wichmann, C., Sigrist, S. J. and Budnik, V. (2006). Nuclear trafficking of Drosophila Frizzled-2 during synapse development requires the PDZ protein dGRIP. *Proc. Natl. Acad. Sci. USA* **103**, 7841-7846.

Ataman, B., Ashley, J., Gorczyca, M., Ramachandran, P., Fouquet, W., Sigrist, S. J. and Budnik, V. (2008). Rapid activity-dependent modifications in synaptic structure and function require bidirectional Wnt signaling. *Neuron* **57**, 705-718.
Beck, E. S., Gasque, G., Imlach, W. L., Jiao, W., Jiwon Choi, B., Wu, P. S., Kraushar, M. L. and McCabe, B. D. (2012). Regulation of Fasciclin II and synaptic terminal development by the splicing factor beag. *J. Neurosci.* **32**, 7058-7073.
Beumer, K. J., Rohrbough, J., Prokop, A. and Broadie, K. (1999). A role for PS integrins in morphological growth and synaptic function at the postembryonic neuromuscular junction of Drosophila. *Development* **126**, 5833-5846.
Beumer, K., Matthies, H. J., Bradshaw, A. and Broadie, K. (2002). Integrins regulate DLG/FAS2 via a CaM kinase II-dependent pathway to mediate synapse elaboration and stabilization during postembryonic development. *Development* **129**, 3381-3391.
Bogdanik, L., Framery, B., Frölich, A., Franco, B., Mornet, D., Bockaert, J., Sigrist, S. J., Grau, Y. and Parmentier, M. L. (2008). Muscle dystroglycan organizes the postsynapse and regulates presynaptic neurotransmitter release at the Drosophila neuromuscular junction. *PLoS ONE* **3**, e2084.
Brand, A. H. and Perrimon, N. (1993). Targeted gene expression as a means of altering cell fates and generating dominant phenotypes. *Development* **118**, 401-415.
Broadie, K., Baumgartner, S. and Prokop, A. (2011). Extracellular matrix and its receptors in Drosophila neural development. *Dev. Neurobiol.* **71**, 1102-1130.
Campbell, R. M., Metzler, M., Granovsky, M., Dennis, J. W. and Marth, J. D. (1995). Complex asparagine-linked oligosaccharides in Mgat1-null embryos. *Glycobiology* **5**, 535-543.
Chapman, E. R. (2002). Synaptotagmin: a Ca(2+) sensor that triggers exocytosis? *Nat. Rev. Mol. Cell Biol.* **3**, 498-508.
Chen, K. and Featherstone, D. E. (2005). Discs-large (DLG) is clustered by presynaptic innervation and regulates postsynaptic glutamate receptor subunit composition in Drosophila. *BMC Biol.* **3**, 1.
Dani, N. and Broadie, K. (2012). Glycosylated synaptomatrix regulation of trans-synaptic signaling. *Dev. Neurobiol.* **72**, 2-21.
Dani, N., Nahm, M., Lee, S. and Broadie, K. (2012). A targeted glycan-related gene screen reveals heparan sulfate proteoglycan sulfation regulates WNT and BMP trans-synaptic signaling. *PLoS Genet.* **8**, e1003031.
Daniels, R. W., Collins, C. A., Gelfand, M. V., Dant, J., Brooks, E. S., Krantz, D. E. and DiAntonio, A. (2004). Increased expression of the Drosophila vesicular glutamate transporter leads to excess glutamate release and a compensatory decrease in quantal content. *J. Neurosci.* **24**, 10466-10474.
Del Grosso, F., De Mariano, M., Passoni, L., Luksch, R., Tonini, G. P. and Longo, L. (2011). Inhibition of N-linked glycosylation impairs ALK phosphorylation and disrupts pro-survival signaling in neuroblastoma cell lines. *BMC Cancer* **11**, 525.
Desai, C. J., Popova, E. and Zinn, K. (1994). A Drosophila receptor tyrosine phosphatase expressed in the embryonic CNS and larval optic lobes is a member of the set of proteins bearing the “HRP” carbohydrate epitope. *J. Neurosci.* **14**, 7272-7283.
DiAntonio, A. (2006). Glutamate receptors at the Drosophila neuromuscular junction. *Int. Rev. Neurobiol.* **75**, 165-179.
DiAntonio, A., Petersen, S. A., Heckmann, M. and Goodman, C. S. (1999). Glutamate receptor expression regulates quantal size and quantal content at the Drosophila neuromuscular junction. *J. Neurosci.* **19**, 3023-3032.
Enneking, E. M., Kudumala, S. R., Moreno, E., Stephan, R., Boerner, J., Godenschwege, T. A. and Pielage, J. (2013). Transsynaptic coordination of synaptic growth, function, and stability by the L1-type CAM Neuroglian. *PLoS Biol.* **11**, e1001537.
Ervasti, J. M., Burwell, A. L. and Geissler, A. L. (1997). Tissue-specific heterogeneity in alpha-dystroglycan sialoglycosylation. Skeletal muscle alpha-dystroglycan is a latent receptor for Vicia villosa agglutinin b4 masked by sialic acid modification. *J. Biol. Chem.* **272**, 22315-22321.
Featherstone, D. E., Rushton, E., Rohrbough, J., Liebl, F., Karr, J., Sheng, Q., Rodesch, C. K. and Broadie, K. (2005). An essential Drosophila glutamate receptor subunit that functions in both central neuropil and neuromuscular junction. *J. Neurosci.* **25**, 3199-3208.
Freeze, H. H. (2006). Genetic defects in the human glycome. *Nat. Rev. Genet.* **7**, 537-551.
Grasa, P., Kaune, H. and Williams, S. A. (2012). Embryos generated from oocytes lacking complex N- and O-glycans have compromised development and implantation. *Reproduction* **144**, 455-465.
Haines, N., Seabrooke, S. and Stewart, B. A. (2007). Dystroglycan and protein O-mannosyltransferases 1 and 2 are required to maintain integrity of Drosophila larval muscles. *Mol. Biol. Cell* **18**, 4721-4730.
Hallermann, S., Kittel, R. J., Wichmann, C., Weyhersmüller, A., Fouquet, W., Mertel, S., Owald, D., Eimer, S., Depner, H., Schwärzel, M. et al. (2010). Naked dense bodies provoke depression. *J. Neurosci.* **30**, 14340-14345.
Hennet, T. (2012). Diseases of glycosylation beyond classical congenital disorders of glycosylation. *Biochim. Biophys. Acta* **1820**, 1306-1317.
Henríquez, J. P. and Salinas, P. C. (2012). Dual roles for Wnt signalling during the formation of the vertebrate neuromuscular junction. *Acta Physiol. (Oxf.)* **204**, 128-136.
Hewitt, J. E. (2009). Abnormal glycosylation of dystroglycan in human genetic disease. *Biochim. Biophys. Acta* **1792**, 853-861.
Humbert, P. O., Grzeschik, N. A., Brumby, A. M., Galea, R., Elsum, I. and Richardson, H. E. (2008). Control of tumourigenesis by the Scribble/Dlg/Lgl polarity module. *Oncogene* **27**, 6888-6907.
Kamimura, K., Ueno, K., Nakagawa, J., Hamada, R., Saitoe, M. and Maeda, N. (2013). Perlecan regulates bidirectional Wnt signaling at the Drosophila neuromuscular junction. *J. Cell Biol.* **200**, 219-233.
Kittel, R. J., Wichmann, C., Rasse, T. M., Fouquet, W., Schmidt, M., Schmid, A., Wagh, D. A., Pawlu, C., Kellner, R. R., Willig, K. I. et al. (2006). Bruchpilot promotes active zone assembly, Ca^{2+} channel clustering, and vesicle release. *Science* **312**, 1051-1054.
Koles, K., Lim, J. M., Aoki, K., Porterfield, M., Tiemeyer, M., Wells, L. and Panin, V. (2007). Identification of N-glycosylated proteins from the central nervous system of Drosophila melanogaster. *Glycobiology* **17**, 1388-1403.
Koles, K., Nunnari, J., Korkut, C., Barria, R., Brewer, C., Li, Y., Leszyk, J., Zhang, B. and Budnik, V. (2012). Mechanism of evenness interrupted (Evi)-exosome release at synaptic boutons. *J. Biol. Chem.* **287**, 16820-16834.
Korkut, C., Ataman, B., Ramachandran, P., Ashley, J., Barria, R., Gherbesi, N. and Budnik, V. (2009). Trans-synaptic transmission of vesicular Wnt signals through Evi/Wntless. *Cell* **139**, 393-404.
Kwon, S. E. and Chapman, E. R. (2012). Glycosylation is dispensable for sorting of synaptotagmin 1 but is critical for targeting of SV2 and synaptophysin to recycling synaptic vesicles. *J. Biol. Chem.* **287**, 35658-35668.
Lahey, T., Gorczyca, M., Jia, X. X. and Budnik, V. (1994). The Drosophila tumor suppressor gene dlg is required for normal synaptic bouton structure. *Neuron* **13**, 823-835.
Lee, H. H., Norris, A., Weiss, J. B. and Frasch, M. (2003). Jelly belly protein activates the receptor tyrosine kinase Alk to specify visceral muscle pioneers. *Nature* **425**, 507-512.
Léonard, R., Rendic, D., Rabouille, C., Wilson, I. B., Préat, T. and Altmann, F. (2006). The Drosophila fused lobes gene encodes an N-acetylglucosaminidase involved in N-glycan processing. *J. Biol. Chem.* **281**, 4867-4875.
Lin, D. M. and Goodman, C. S. (1994). Ectopic and increased expression of Fasciclin II alters motoneuron growth cone guidance. *Neuron* **13**, 507-523.
Littleton, J. T., Bellen, H. J. and Perin, M. S. (1993). Expression of synaptotagmin in Drosophila reveals transport and localization of synaptic vesicles to the synapse. *Development* **118**, 1077-1088.
Long, A. A., Kim, E., Leung, H. T., Woodruff, E., 3rd, An, L., Doerge, R. W., Pak, W. L. and Broadie, K. (2008). Presynaptic calcium channel localization and calcium-dependent synaptic vesicle exocytosis regulated by the Fuseless protein. *J. Neurosci.* **28**, 3668-3682.
Long, A. A., Mahapatra, C. T., Woodruff, E. A., 3rd, Rohrbough, J., Leung, H. T., Shino, S., An, L., Doerge, R. W., Metzstein, M. M., Pak, W. L. et al. (2010). The nonsense-mediated decay pathway maintains synapse architecture and synaptic vesicle cycle efficacy. *J. Cell Sci.* **123**, 3303-3315.
Marqués, G. (2005). Morphogens and synaptogenesis in Drosophila. *J. Neurobiol.* **64**, 417-434.
Marrus, S. B., Portman, S. L., Allen, M. J., Moffat, K. G. and DiAntonio, A. (2004). Differential localization of glutamate receptor subunits at the Drosophila neuromuscular junction. *J. Neurosci.* **24**, 1406-1415.
Martin, P. T. (2003). Glycobiology of the neuromuscular junction. *J. Neurocytol.* **32**, 915-929.
McCabe, B. D., Marqués, G., Haghighi, A. P., Fetter, R. D., Crotty, M. L., Haerry, T. E., Goodman, C. S. and O’Connor, M. B. (2003). The BMP homolog Gbb provides a retrograde signal that regulates synaptic growth at the Drosophila neuromuscular junction. *Neuron* **39**, 241-254.
Müller, M. and Davis, G. W. (2012). Transsynaptic control of presynaptic Ca^{2+} influx achieves homeostatic potentiation of neurotransmitter release. *Curr. Biol.* **22**, 1102-1108.
Muntoni, F., Torelli, S. and Brockington, M. (2008). Muscular dystrophies due to glycosylation defects. *Neurotherapeutics* **5**, 627-632.
Nahm, M., Long, A. A., Paik, S. K., Kim, S., Bae, Y. C., Broadie, K. and Lee, S. (2010). The Cdc42-selective GAP rich regulates postsynaptic development and retrograde BMP transsynaptic signaling. *J. Cell Biol.* **191**, 661-675.
Nahm, M., Lee, M. J., Parkinson, W., Lee, M., Kim, H., Kim, Y. J., Kim, S., Cho, Y. S., Min, B. M., Bae, Y. C. et al. (2013). Spartin regulates synaptic growth and neuronal survival by inhibiting BMP-mediated microtubule stabilization. *Neuron* **77**, 680-695.
Nakamura, N., Stalnaker, S. H., Lyalin, D., Lavrova, O., Wells, L. and Panin, V. M. (2010). Drosophila Dystroglycan is a target of O-mannosyltransferase activity of two protein O-mannosyltransferases, Rotated Abdomen and Twisted. *Glycobiology* **20**, 381-394.
Ohshiro, T., Yagami, T., Zhang, C. and Matsuzaki, F. (2000). Role of cortical tumour-suppressor proteins in asymmetric division of Drosophila neuroblast. *Nature* **408**, 593-596.
Paschinger, K., Rendić, D. and Wilson, I. B. (2009). Revealing the anti-HRP epitope in Drosophila and Caenorhabditis. *Glycoconj. J.* **26**, 385-395.
Patton, B. L. (2003). Basal lamina and the organization of neuromuscular synapses. *J. Neurocytol.* **32**, 883-903.
Pownall, S., Kozak, C. A., Schappert, K., Sarkar, M., Hull, E., Schachter, H. and Marth, J. D. (1992). Molecular cloning and characterization of the mouse UDP-N-acetylglucosamine:alpha-3-D-mannoside beta-1,2-N-acetylglucosaminyltransferase I gene. *Genomics* **12**, 699-704.
Puthalakath, H., Burke, J. and Gleeson, P. A. (1996). Glycosylation defect in Lec1 Chinese hamster ovary mutant is due to a point mutation in N-acetylglucosaminyltransferase I gene. *J. Biol. Chem.* **271**, 27818-27822.
Qin, G., Schwarz, T., Kittel, R. J., Schmid, A., Rasse, T. M., Kappei, D., Ponimaskin, E., Heckmann, M. and Sigrist, S. J. (2005). Four different subunits are essential for expressing the synaptic glutamate receptor at neuromuscular junctions of Drosophila. *J. Neurosci.* **25**, 3209-3218.
Rendić, D., Sharrow, M., Katoh, T., Overcarsh, B., Nguyen, K., Kapurch, J., Aoki, K., Wilson, I. B. and Tiemeyer, M. (2010). Neural-specific α3-fucosylation of N-

linked glycans in the Drosophila embryo requires fucosyltransferase A and influences developmental signaling associated with O-glycosylation. *Glycobiology* **20**, 1353-1365.
Richmond, J. E. and Broadie, K. S. (2002). The synaptic vesicle cycle: exocytosis and endocytosis in Drosophila and C. elegans. *Curr. Opin. Neurobiol.* **12**, 499-507.
Rohrbough, J. and Broadie, K. (2002). Electrophysiological analysis of synaptic transmission in central neurons of Drosophila larvae. *J. Neurophysiol.* **88**, 847-860.
Rohrbough, J. and Broadie, K. (2010). Anterograde Jelly belly ligand to Alk receptor signaling at developing synapses is regulated by Mind the gap. *Development* **137**, 3523-3533.
Rohrbough, J., Rushton, E., Woodruff, E., 3rd, Fergestad, T., Vigneswaran, K. and Broadie, K. (2007). Presynaptic establishment of the synaptic cleft extracellular matrix is required for post-synaptic differentiation. *Genes Dev.* **21**, 2607-2628.
Rohrbough, J., Kent, K. S., Broadie, K. and Weiss, J. B. (2013). Jelly Belly trans-synaptic signaling to anaplastic lymphoma kinase regulates neurotransmission strength and synapse architecture. *Dev. Neurobiol.* **73**, 189-208.
Rushton, E., Rohrbough, J. and Broadie, K. (2009). Presynaptic secretion of mind-the-gap organizes the synaptic extracellular matrix-integrin interface and postsynaptic environments. *Dev. Dyn.* **238**, 554-571.
Rushton, E., Rohrbough, J., Deutsch, K. and Broadie, K. (2012). Structure-function analysis of endogenous lectin mind-the-gap in synaptogenesis. *Dev. Neurobiol.* **72**, 1161-1179.
Sarkar, M., Leventis, P. A., Silvescu, C. I., Reinhold, V. N., Schachter, H. and Boulianne, G. L. (2006). Null mutations in Drosophila N-acetylglucosaminyltransferase I produce defects in locomotion and a reduced life span. *J. Biol. Chem.* **281**, 12776-12785.
Sarkar, M., Iliadi, K. G., Leventis, P. A., Schachter, H. and Boulianne, G. L. (2010). Neuronal expression of Mgat1 rescues the shortened life span of Drosophila Mgat11 null mutants and increases life span. *Proc. Natl. Acad. Sci. USA* **107**, 9677-9682.
Schachter, H. (2010). Mgat1-dependent N-glycans are essential for the normal development of both vertebrate and invertebrate metazoans. *Semin. Cell Dev. Biol.* **21**, 609-615.
Schachter, H. and Boulianne, G. (2011). Life is sweet! A novel role for N-glycans in Drosophila lifespan. *Fly (Austin)* **5**, 18-24.
Shi, S., Williams, S. A., Seppo, A., Kurniawan, H., Chen, W., Ye, Z., Marth, J. D. and Stanley, P. (2004). Inactivation of the Mgat1 gene in oocytes impairs oogenesis, but embryos lacking complex and hybrid N-glycans develop and implant. *Mol. Cell. Biol.* **24**, 9920-9929.
Staples, J. and Broadie, K. (2013). The cell polarity scaffold Lethal Giant Larvae regulates synapse morphology and function. *J. Cell Sci.* **126**, 1992-2003.
Stevens, R. J., Akbergenova, Y., Jorquera, R. A. and Littleton, J. T. (2012). Abnormal synaptic vesicle biogenesis in Drosophila synaptogyrin mutants. *J. Neurosci.* **32**, 18054-18067.
Sun, M. and Xie, W. (2012). Cell adhesion molecules in Drosophila synapse development and function. *Sci. China Life Sci.* **55**, 20-26.
Tanaka, K., Kitagawa, Y. and Kadowaki, T. (2002). Drosophila segment polarity gene product porcupine stimulates the posttranslational N-glycosylation of wingless in the endoplasmic reticulum. *J. Biol. Chem.* **277**, 12816-12823.
Tang, X., Wu, Y., Belenkaya, T. Y., Huang, Q., Ray, L., Qu, J. and Lin, X. (2012). Roles of N-glycosylation and lipidation in Wg secretion and signaling. *Dev. Biol.* **364**, 32-41.
Thomas, U. and Sigrist, S. J. (2012). Glutamate receptors in synaptic assembly and plasticity: case studies on fly NMJs. *Adv. Exp. Med. Biol.* **970**, 3-28.
Tran, D. T., Lim, J. M., Liu, M., Stalnaker, S. H., Wells, L., Ten Hagen, K. G. and Live, D. (2012). Glycosylation of α-dystroglycan: O-mannosylation influences the subsequent addition of GalNAc by UDP-GalNAc polypeptide N-acetylgalactosaminyltransferases. *J. Biol. Chem.* **287**, 20967-20974.
Wagh, D. A., Rasse, T. M., Asan, E., Hofbauer, A., Schwenkert, I., Dürrbeck, H., Buchner, S., Dabauvalle, M. C., Schmidt, M., Qin, G. et al. (2006). Bruchpilot, a protein with homology to ELKS/CAST, is required for structural integrity and function of synaptic active zones in Drosophila. *Neuron* **49**, 833-844.
Wairkar, Y. P., Fradkin, L. G., Noordermeer, J. N. and DiAntonio, A. (2008). Synaptic defects in a Drosophila model of congenital muscular dystrophy. *J. Neurosci.* **28**, 3781-3789.
Wang, T., Liu, Y., Xu, X. H., Deng, C. Y., Wu, K. Y., Zhu, J., Fu, X. Q., He, M. and Luo, Z. G. (2011). Lgl1 activation of rab10 promotes axonal membrane trafficking underlying neuronal polarization. *Dev. Cell* **21**, 431-444.
Ye, Z. and Marth, J. D. (2004). N-glycan branching requirement in neuronal and postnatal viability. *Glycobiology* **14**, 547-558.
Zinsmaier, K. E., Hofbauer, A., Heimbeck, G., Pflugfelder, G. O., Buchner, S. and Buchner, E. (1990). A cysteine-string protein is expressed in retina and brain of Drosophila. *J. Neurogenet.* **7**, 15-29.